

Haptic Pottery Modeling Using Circular Sector Element Method

Jaebong Lee, Gabjong Han, and Seungmoon Choi

Haptics and Virtual Reality Laboratory
Department of Computer Science and Engineering
POSTECH, Republic of Korea
`{novaever, hkj84, choism}@postech.ac.kr`

Abstract. This paper presents an efficient modeling system of virtual pottery in which the user can deform a body of virtual clay with a haptic tool. The clay body is represented with a set of circular sector elements based on the cylindrical symmetry of pottery. The circular sector element method allows much finer spatial resolution for modeling than previous techniques. Also described are efficient algorithms for collision detection and response where the viscosity of virtual clay is simulated along with the friction due to the rotating potter's wheel. Empirical evaluation showed that the modeling system is computationally efficient, is intuitive to use, and provides convincing model deformation and force feedback.

Keywords: Pottery modeling, virtual clay, haptic rendering, deformable object, circular sector element method, cultural heritage.

1 Introduction

Making pottery from clay rotating on a potter's wheel is one of the most common worldwide cultural heritages. There have been consistent research interests in modeling systems for virtual clay or pottery. Early research included tactile feedback using vibration motors as a metaphor of virtual contact [1][2]. A force-reflecting haptic interface soon took over the place and was used in several studies for tangible modeling [3][4][5][6].

Our research aims at constructing a high-fidelity *haptic pottery modeling system* with faster and more efficient algorithm than the previous methods. The system features with a *Circular Sector Element Method (CSEM)* where pottery is modeled with a set of circular sector elements based on its cylindrical symmetry. The CSEM allows efficient collision detection and response algorithms for model deformation and force rendering. Our empirical evaluation showed that the CSEM is quite effective in terms of both modeling resolution and computational performance, allowing the 1 kHz haptic update rate for very dense pottery models. With our system, the user can easily experience making pottery in a virtual environment using a force-feedback haptic interface.

2 Pottery Model Using Circular Sector Elements

In our virtual pottery modeling system, pottery is represented using a number of circular sector elements as illustrated in Figure 1. The basic idea behind the CSEM is that pottery is cylindrically symmetric and mostly deformed along the radial direction due to the potter's wheel. Thus, using the circular sector elements can be one of the most natural candidates for modeling virtual pottery. The CSEM shares the same idea with the LEM [7][8]; the LEM allows model deformation along the longitudinal direction only, whereas the CSEM along the radial direction only. As will become apparent soon, the CSEM leads to high-fidelity modeling of virtual pottery with a relatively small number of elements and to efficient collision detection and response algorithms.

Notations for the CSEM are defined in Figure 2, and will be used throughout this paper. The model representing a body of virtual clay is placed on the horizontal plane and a spherical haptic tool for clay deformation is on the right side of the figure. A circular sector element is denoted by $\mathbf{S}^i = (S_r^i, S_\theta^i, S_h^i)$ using the cylindrical coordinates of the end-point of \mathbf{S}^i . The index i will be dropped for simplicity whenever appropriate. The Haptic Interaction Point (HIP) position, the radius of the HIP sphere, and the distance between the HIP and the y -axis are represented by \mathbf{H} , H_r , and d , respectively. The Cartesian coordinates of a vector such as $\mathbf{X} = (X_x, X_y, X_z)$ will also be used in the paper. Note that the CSEM is a boundary representation; we do not explicitly model the internal volume.

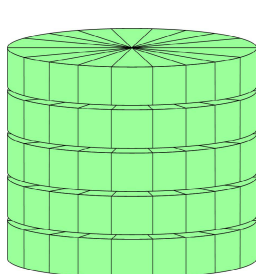


Fig. 1. Pottery model composed of circular sector elements

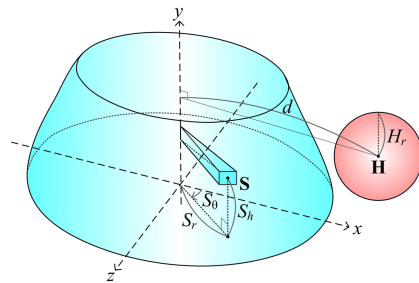


Fig. 2. Definitions of a coordinate frame and related symbols

3 Collision Detection

In the CSEM, pottery can be deformed from outside to inside (contraction mode) or from inside to outside (expansion mode). Collision detection and response algorithms for the two modes are symmetric. Thus, we first describe the algorithms for the contraction mode, followed by changes necessary for the expansion mode.

Collision detection between a pottery model and the HIP sphere consists of three steps. First, a set of circular sector elements that can be possibly in contact

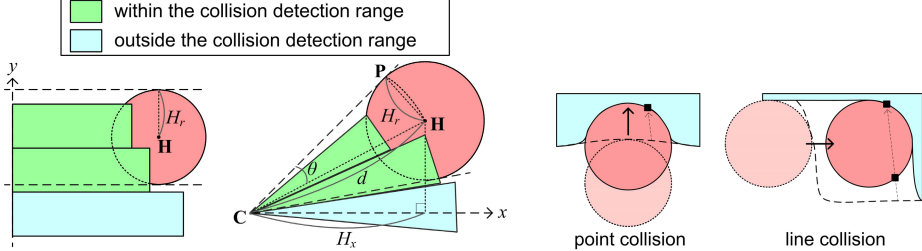


Fig. 3. Ranges for collision in the height direction (left) and the radial direction (right)

Fig. 4. Illustration of point collision (left) and line collision (right)

with the HIP sphere are selected and passed to steps 2 and 3. Second, one of two collision types is assigned to each element passed from step 1. Finally, each element goes through a collision test appropriate to its collision type. The three steps are described in details in the rest of this section.

In step 1, we select, given the HIP position \mathbf{H} , the elements \mathbf{S}^i that satisfy both of the two necessary conditions in (1) and (2) (also see Figure 3).

$$S_h^i \in [H_y - H_r, H_y + H_r] . \quad (1)$$

$$S_\theta^i \in \left[\cos^{-1}\left(\frac{H_x}{d}\right) - \frac{H_r}{d}, \cos^{-1}\left(\frac{H_x}{d}\right) + \frac{H_r}{d} \right] . \quad (2)$$

In (2), the central angle θ of the circular sector \mathbf{CHP} is approximated to H_r/d under the assumption that θ is sufficiently small such that the arc length of \mathbf{HP} and H_r are almost the same. In implementation, the ranges in (1) and (2) can be mapped to the corresponding index ranges of \mathbf{S}^i in $O(1)$ time.

In step 2, two collision types are considered (see Figure 4). In point collision (left figure), a collision occurs at the end-point of an element that will be consequently deformed in the radial direction. In line collision (right figure), the HIP touches the side of an element, and deformation proceeds in the tangential direction. Type decision is simple: An element \mathbf{S} can be in point collision if $S_r < d$ (see Figure 5). Otherwise, \mathbf{S} can be in line collision. In Figure 5, \mathbf{S}^1 can be in point collision whereas \mathbf{S}^2 can be in line collision.

In step 3, each element is checked for collision using the collision test of its type. This is explained with Figure 5. In the figure, \mathbf{C} is the point on the y -axis at the height of an element \mathbf{S} , and r is the radius of the cross-section between the HIP sphere and the xz plane at the height of \mathbf{S} . A line joining \mathbf{C} and \mathbf{S} intersects the cross-section at two points, \mathbf{E}_1 and \mathbf{E}_2 , with \mathbf{E}_1 being a nearer point to \mathbf{C} . A point collision can be detected by comparing S_r and the distance between \mathbf{C} and \mathbf{E}_1 (see \mathbf{S}_1). In case of a line collision, the middle point of \mathbf{E}_1 and \mathbf{E}_2 , \mathbf{M} , should lie inside the cross-section of the HIP sphere (see \mathbf{S}_2). Therefore, we judge that element \mathbf{S} is in contact with the HIP sphere if the penetration depth $p > 0$, where

$$p = \begin{cases} S_r - \|\mathbf{E}_1 - \mathbf{C}\| & \text{(For point collision)} \\ r - \|\mathbf{H} - \mathbf{M}\| & \text{(For line collision)} \end{cases} . \quad (3)$$

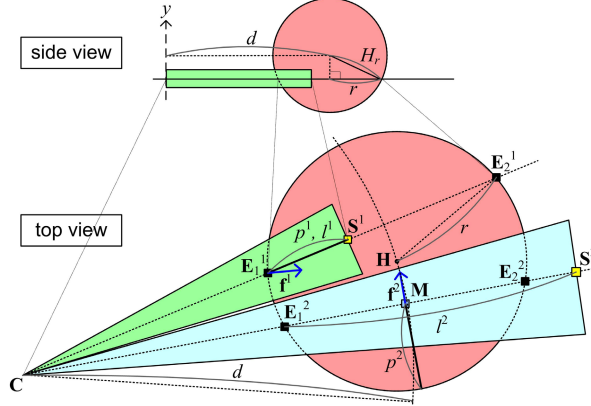


Fig. 5. Side and top views of the pottery model

To use the collision detection algorithm for the expansion mode, only minor changes in steps 2 and 3 are necessary. In step 2, \mathbf{S} can be in point collision if $S_r > d$ and in line collision otherwise, unlike the contraction mode. In step 3, the penetration depth computation for point collision needs to be replaced with

$$p = \|\mathbf{E}_2 - \mathbf{C}\| - S_r . \quad (4)$$

4 Collision Response

In this section, we explain how adequate deformation and rendering force are computed for each circular sector element touched by the HIP sphere.

4.1 Deformation

The deformation algorithm is based on the well-known physics that stress is proportional to viscosity and the time derivative of strain. If an element \mathbf{S} is in contact with the HIP sphere, its radius S_r needs to be decreased by l for the element to be untouched, i.e., for \mathbf{S} to be at \mathbf{E}_1 (see Figure 5). Thus, l can be assumed to be proportional to stress applied to the element. We control the rate of change ΔS_r with a pseudo viscosity coefficient c_η , as follows:

$$l = S_r - \|\mathbf{E}_1 - \mathbf{C}\| . \quad (5)$$

$$\Delta S_r = -\frac{l}{c_\eta} . \quad (6)$$

This deformation is computed for each colliding element and applied to its radius. In the expansion mode, \mathbf{E}_1 in (5) should be replaced with \mathbf{E}_2 .

4.2 Force Feedback

Let \mathbf{F}_v^i be the resistance force due to a contact with an element \mathbf{S}_i and \mathbf{F}_r be the frictional force due to the rotation of a pottery model. Then the total feedback force \mathbf{F} can be computed by summing up \mathbf{F}_v^i and \mathbf{F}_r as follows:

$$\mathbf{F} = \sum_i \mathbf{F}_v^i + \mathbf{F}_r . \quad (7)$$

For each contacting element \mathbf{S}_i , \mathbf{F}_v^i is determined as follows. Let \mathbf{f}^i in Figure 5 be a unit vector pointing to the reverse direction of HIP penetration such that:

$$\mathbf{f}^i = \begin{cases} \frac{\mathbf{H}-\mathbf{E}_1^i}{\|\mathbf{H}-\mathbf{E}_1^i\|} & \text{(For point collision)} \\ \frac{\mathbf{H}-\mathbf{M}^i}{\|\mathbf{H}-\mathbf{M}^i\|} & \text{(For line collision)} \end{cases} . \quad (8)$$

Also, let c_v be the coefficient of resistance. Under the proportional relationship between the deformation length and the force, the resistance force is :

$$\mathbf{F}_v^i = c_v p^i \mathbf{f}^i . \quad (9)$$

Moreover, the frictional force is generated if the user deforms a rotating pottery model. Let c_r be the coefficient of friction and \mathbf{t} be the unit tangential vector in the rotation direction. We compute the friction force simply as:

$$\mathbf{F}_r = c_r \max_i (p^i) \mathbf{t} , \quad (10)$$

using the maximum penetration depth as a measure of normal force applied to the pottery by the HIP sphere.

In the expansion mode, the only necessary change is to replace \mathbf{E}_1 in (8) with \mathbf{E}_2 .

5 Performance Evaluation

Our pottery modeling system was implemented on a commodity desktop PC (Intel Pentium 4 3.2GHz CPU, 1.00GB RAM, and NVIDIA Geforce 8800 GTS graphics card) using a PHANToM Omni device (Sensable Technology, Inc.) as a force-feedback interface. The user can control the rotating speed of the potter's wheel using a keyboard and deform virtual pottery using the Omni stylus. Several participants who used the modeling system reported that it provided easy and intuitive interface for virtual pottery modeling. Several examples designed with the system are provided in Figure 6. These examples show the flexibility of our system.

We measured the computational performance of the modeling system. For this, model resolution was defined as a combination of the number of thin cylinders in the height direction and that of circular sectors on the horizontal plane. Four levels of model resolution, 36,000 (200×180), 72,000 (200×360), 144,000

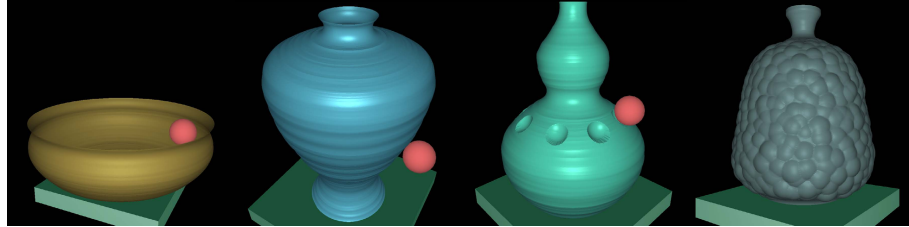


Fig. 6. Various pottery models designed with our system

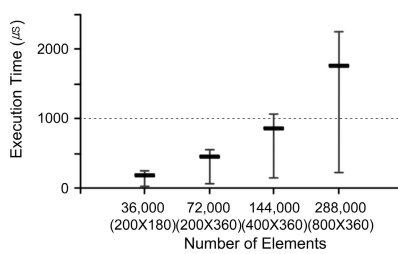


Fig. 7. Execution times for one rendering loop under various model resolutions. The model resolution is written in a form, $(n_h \times n_r)$, where n_h represents the number of elements in the height direction and n_r that in the angular direction.

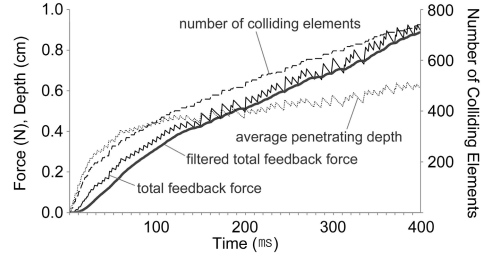


Fig. 8. The number of colliding elements, average penetrating depth, total feedback force, and filtered total feedback force using low-pass filter recorded while the HIP sphere slowly pushed into a pottery model

(400×360), and 288,000 (800×360), were tested, and the results are summarized in Figure 7. Recall that the execution time of collision detection and response in our modeling system is proportional to the number of circular sector elements that passed the collision range test in step 1. Given the radius of the HIP sphere, the number of such elements linearly increases with the numbers of elements in the height and angular directions. Moreover, it is inversely proportional to the distance of the HIP from the center axis (d in Figure 5), that is, the closer the HIP is to the center axis, the slower the computation is. Such variability is represented by intervals in Figure 7 with averages marked with thick bars in the figure. Overall, the system achieved the 1 kHz update rate until the model resolution was raised to 400×360 . With this resolution, we can render a 7.2 cm tall pottery model with 0.18 mm height resolution and 1° angular resolution, which is quite dense (recall that the position sensing resolution of the PHANTOM Omni is about 0.055 mm).

The stability of haptic rendering was also examined. In our algorithm, some circular sector elements that are used for force computation in the current rendering loop might be excluded in the next rendering loop. This can adversely affect the smoothness of total force change in (7). To circumvent rendering instability, we used a Butterworth low-pass filter with a 10Hz cutoff frequency.

Through extensive testing, we confirmed that our modeling system does not accompany rendering instability, as shown in Figure 8. It can be seen that despite the jagged penetration depth, the filtered feedback force was quite smooth.

6 Conclusions

The central idea of this paper has been utilizing the cylindrical symmetry of pottery, which resulted in a very efficient model and algorithms named the circular sector element method. We showed that a model composed of the tens of thousands of elements could be stably simulated in real time, keeping the fast haptic update rate of 1 kHz.

At present, the haptic tool for deformation is modeled by a sphere for the simplicity of collision detection and response computation, but we noticed that this limits the types of decorations that can be made on the pottery surface. We thus plan to extend the algorithms to support various tool shapes in the future. We also plan to conduct a formal usability study.

Acknowledgments. This work was supported in parts by a grant No. R01-2006-000-10808-0 from the Korea Science and Engineering Foundation (KOSEF) funded by the Korea government (MOST) and by the Brain Korea 21 program from the Korea Research Foundation.

References

1. Kameyama, K.: Virtual clay modeling system. In: Proceedings of the ACM Symposium on Virtual Reality Software and Technology, pp. 197–200 (1997)
2. Korida, K., Nishino, H., Utsumiya, K.: An interactive 3D interface for a virtual ceramic art work environment. In: Proceedings of the 1997 International Conference on Virtual Systems and MultiMedia, pp. 227–234 (1997)
3. Massie, T.: A tangible goal for 3D modeling. IEEE Computer Graphics & Applications 18(3), 62–65 (1998)
4. Chai, Y., Luecke, G.R., Edwards, J.C.: Virtual clay modeling using the ISU exoskeleton. In: Proceedings of IEEE Virtual Reality Annual International Symposium, pp. 76–80 (1998)
5. McDonnell, K.T., Qin, H., Wlodarczyk, R.A.: Virtual clay: A real-time sculpting system with haptic toolkits. In: Proceedings of the Symposium on Interactive 3D Graphics, pp. 179–190 (2001)
6. Han, G., Kim, J., Choi, S.: Virtual pottery modeling with force feedback using cylindrical element method. In: Proceedings of the International Conference on Next-Generation Computing, pp. 125–129 (2007)
7. Costa, I.F., Balaniuk, R.: LEM - an approach for real time physically based soft tissue simulation. In: Proceedings of IEEE International Conference on Robotics and Automation, pp. 2337–2343 (2001)
8. Sundaraj, K., Laugier, C., Costa, I.F.: An approach to LEM modeling: Construction, collision detection and dynamic simulation. In: Proceedings of IEEE/RSJ International Conference on Intelligent Robots and Systems, pp. 2196–2201 (2001)